THE JOURNAL OF PHYSICAL CHEMISTRY C

Article

pubs.acs.org/JPCC

Dynamics of Ion Binding to Graphene Nanostructures

Niladri Patra,[†] Dominic A. Esan,[†] and Petr Král*[,†,‡]

[†]Department of Chemistry and [‡]Department of Physics, University of Illinois at Chicago, Chicago, Illinois 60607, United States

Web-Enhanced Feature

ABSTRACT: We model the dynamics of ion binding to graphene nanostructures. In order to disclose the likely ion binding dynamics, we first perform scanned single-point DFT calculations of monovalent ions (Na^+, Li^+, Cl^-, F^-) at fixed distances above planar graphene-like H-passivated molecules of different shapes and sizes. The scans reveal intriguing details about the ion-nanostructure potential energy and charge transfer surfaces. We correlate these static results with our room-temperature quantum molecular dynamics simulations of the ion−molecule systems, performed in both vacuum and water. Our simulations show that anions either are physisorbed onto the nanostructures or covalently bind at their selected regions, depending on the initial conditions, while cations only physisorb onto them.

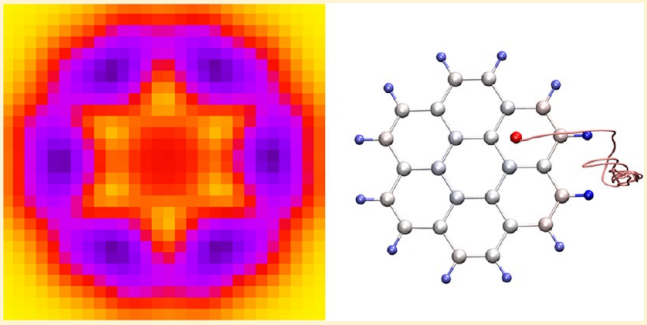

1. INTRODUCTION

Since its recent isolation,[1] graphene was the subject of many exciting experimental[2,3] and theoretical studies.[4] In particular, chemically functionalized graphene[5−8] can have unique properties and potential applications.[9−11] Large attention was devoted to graphene oxidation,[12,13] sulfonation,[14] hydrogenation,[15−18] fluorination,[19−25] and chlorination.[26−29] Although, F^- was shown to bind covalently to graphene, Cl^- can either bind covalently or physisorb on it.[26,27] Functionalized graphene nanostructures, such as nanoribbons[30] and porous graphene,[31] have also been studied for their many potential applications in electronics,[32−34] molecular filtration,[35] and nanofluidics.[36−38]

However, it may be difficult to precisely functionalize graphene nanostructures since they are highly polarizable and they can have locally very different chemistries. Detailed information about their chemistry could be obtained in refined experiments. Recently, atomic force microscopy was used to map subtle differences in bond length and charge density connected with nonequivalent C−C bonds in polycyclic aromatic hydrocarbons.[39] Alternatively, advanced simulations could be used to guide experiments aiming at precise functionalization of various graphene nanostructures.

With this in mind, we model the dynamics of ion−nanostructure binding. We first use TeraChem[40] to perform scanned single-point DFT calculations of monovalent ions (Na^+, Li^+, Cl^-, F^-) at fixed distances above planar carbon-based H-passivated molecules of different shapes and sizes. At each point, we calculate the ion−nanostructure interaction energy and charge transfer (Mulliken charges considered). In principle, the scans can be performed at finite temperatures and averaged over a thermal ensemble to predict the binding dynamics of the components. We compare these results with separate quantum molecular dynamics simulations of the ion−molecule binding dynamics.

2. COMPUTATIONAL METHODS

The single-point energy calculations and molecular dynamical simulations were done for cations (Na^+, Li^+) at the B3LYP/3-21g* level, with dispersion corrections (DFT-D3),[41,42] while for anions (F^-, Cl^-) they were done at the RHF/3-21g level, due to stability reasons. The use of B3LYP and the relatively small systems studied helps to minimize the self-interaction error in DFT.[43] We used the Conjugate Gradient (CG) method,[44] the convergence criterion on a total energy of 10^{-6}, an X-matrix tolerance of 10^{-4}, a wave function convergence threshold of 3.0×10^{-5}, and the dispersion corrections.[41,42] Our test calculations of the systems with other DFT methods (ωPBE, ωB97, ωB97x, and camB3LYP) gave similar results.

In the MD simulations (T = 100 and 300 K), we used the Langevin dynamics with a damping coefficient of γ_{Lang} = 1 ps^{-1} and a time step of 1 fs (no periodic boundary conditions). Given the large power of TeraChem, we can scan the structures at a relatively large pixel density of 0.5 Å (0.25 Å for the edge passage), giving in each scan a picture with ≈700 pixels.

3. RESULTS AND DISCUSSION

3.1. Coronene ($C_{24}H_{12}$). In Figure 1, we present the potential energy (top) and ion charge (middle) scans obtained for coronene. The scans were performed at a height of h = 2 Å for F^- (left) and h = 2.5 Å for Na^+ (right) above the optimized coronene (Figures 1c and f), using the RHF/3-21g and B3LYP/3-21g* levels of theory, respectively.

Figure 1a reveals that the potential energy surface for F^- has a pronounced C_6 symmetry. The coupling energy is large

Received: January 24, 2013
Revised: March 25, 2013
Published: March 26, 2013

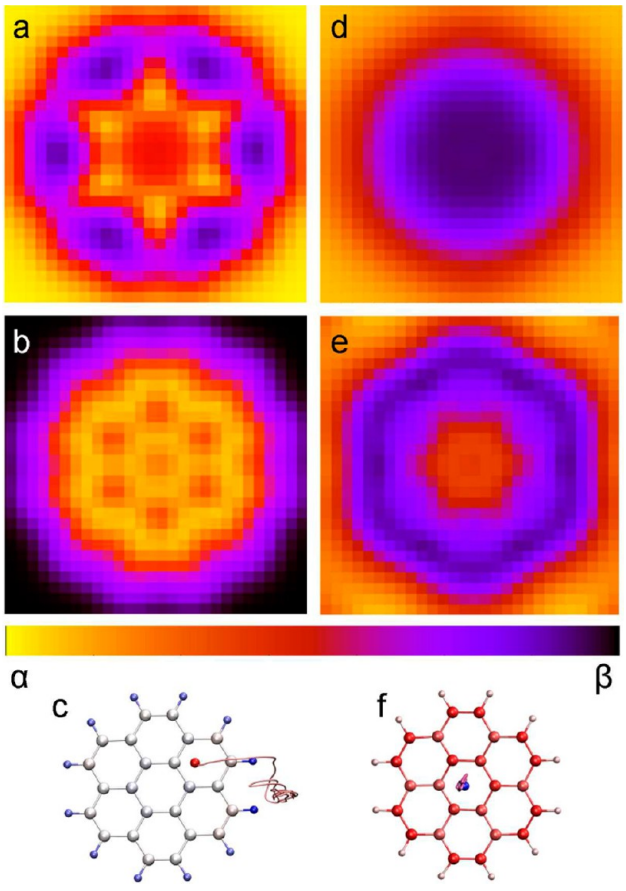

Figure 1. Scanning of F^- (left) and Na^+ (right) ions coupled to coronene, evaluated at h = 2 Å (for F^-) and 2.5 Å (for Na^+) above its surface. The potential energy surface for (a) F^- (α = −1009.60 au and β = −1009.64 au) and (d) Å Na^+ (α = −1077.97 au and β = −1078.06 au). The charge transfer surface for (b) F^- (α = −0.65 and β = −1) and (e) Na^+ (α = 1 and β = 0.8). The dynamics of (c) F^- released at h = 4 Å (T = 100 K) and (f) Na^+ released at h = 3.5 Å above the coronene flake (T = 300 K). The flakes are shown for the last simulation frame, where atoms are colored by charge (see movies 1, 2, and 3). (a–f) have the same scale. The pixel density is 0.5 Å.

between the H atoms of neighboring C rings at the zigzag edges of coronene, and it is small in its central region, giving a maximum energy difference of 1.6 eV (see scale). This can be explained by a large average positive charge on the H atoms of q_H = −0.25 e (q_C = 0.14 e). The charge transfer distribution in Figure 1b shows that the transfer is large (0.35 e) above the carbon atoms. From the binding energy profile, we expect that the area around the edge H atoms is the most likely target for F^- binding.

We compare these predictions with the simulated trajectories of F^- released at different heights above the coronene. When F^- is released at h = 4 Å, at a temperature of T = 100 K, it moves to the coronene periphery and reaches it within 2.5 ps (see movie 2), as seen in Figure 1c. Over there it Coulombically couples (physisorption) to the polarized coronene and stays between two adjacent H atoms of the neighboring C rings, within 2.6 Å from each of them. When these simulations are repeated at T = 300 K, the ion moves along a slightly longer path and again couples to the two H atoms. However, when F^- is released at h < 3.5 Å above the coronene center (T = 300 K), it binds covalently to one of the closest C atoms with a bond length of 1.35 Å (see movie 1). When the room-temperature simulations are performed at h = 4 Å in (nonpolarized) water (B3LYP/6-31g), F^- is stabilized within 4 Å from the edge H atoms.

We also performed the scans for cations. Figure 1d shows that Na^+ coupling is weak and of a radial symmetry in the negatively charged coronene center (q_C = 0.12 e, q_H = −0.22 e), indicating a tendency to physisorption. The charge transfer (Figure 1e) is larger in the peripheral region and of a clear C_6 symmetry. When Na^+ is released at h = 3.5 Å (T = 300 K), it diffuses around the coronene center (physisorb) at an average height of h = 2.5 Å, as shown on the (1 ps) trajectory in Figure 1f (see movie 3). In water at T = 300 K, Na^+ diffuses at h = 3.5 Å above the coronene center (B3LYP/6-31g).

3.2. Triangular Graphene Flakes. We also want to understand the binding dynamics of ions to other graphene nanostructures. Therefore, we model the ion binding to triangular H-passivated graphene flakes with zigzag and armchair edges of different sizes, as shown in Figures 2c and f, respectively (RHF/3-21g level). Figure 2a shows the potential energy of F^- evaluated at h = 2 Å above the zigzag-edge flake. It has a clear preference (4.9 eV) for the edge carbons. Figure 2b indicates that large charge transfers (0.5 e) occur along the flake

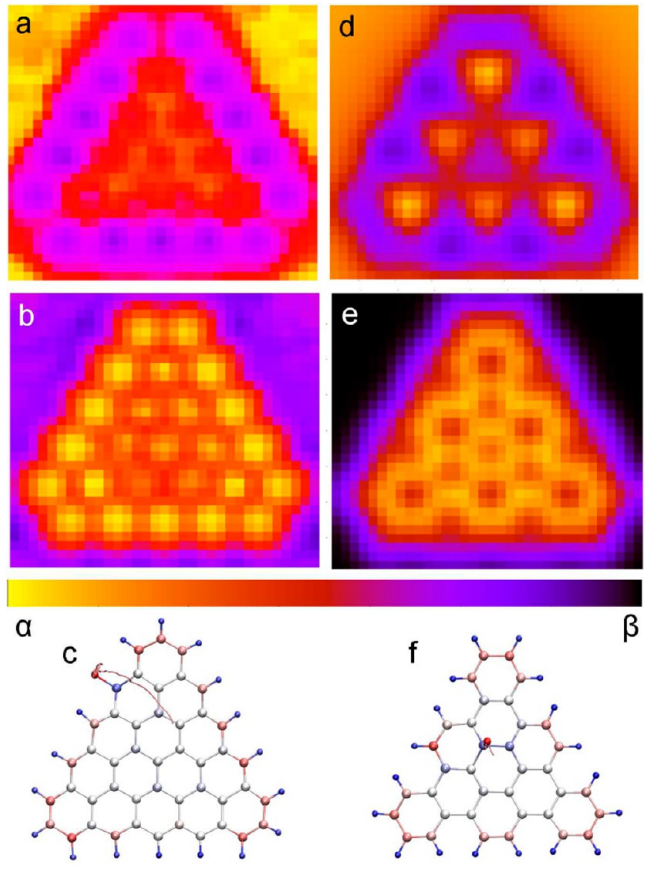

Figure 2. Scanning of the F^- ion coupled to zigzag-edge (left) and armchair-edge (right) triangular graphene flakes, evaluated at h = 2 Å above their surfaces. The potential energy surface for (a) zigzag (α = −1841.36 au and β = −1841.54 au) and (d) armchair (α = −1464.97 au and β = −1465.04 au) flakes. The charge transfer surface for (b) zigzag (α = −0.45 and β = −0.95) and (e) armchair (α = −0.65 and β = −1) flakes. The structure and dynamics of (c) zigzag flake after 1 ps simulations with F^- released at h = 4.8 Å (see movie 4) and (f) armchair flake in 0.4 ps simulations where F^- released at h = 3.6 Å. The covalent coupling formed is seen in both cases.

dx.doi.org/10.1021/jp400835w | J. Phys. Chem. C 2013, 117, 10750–10754

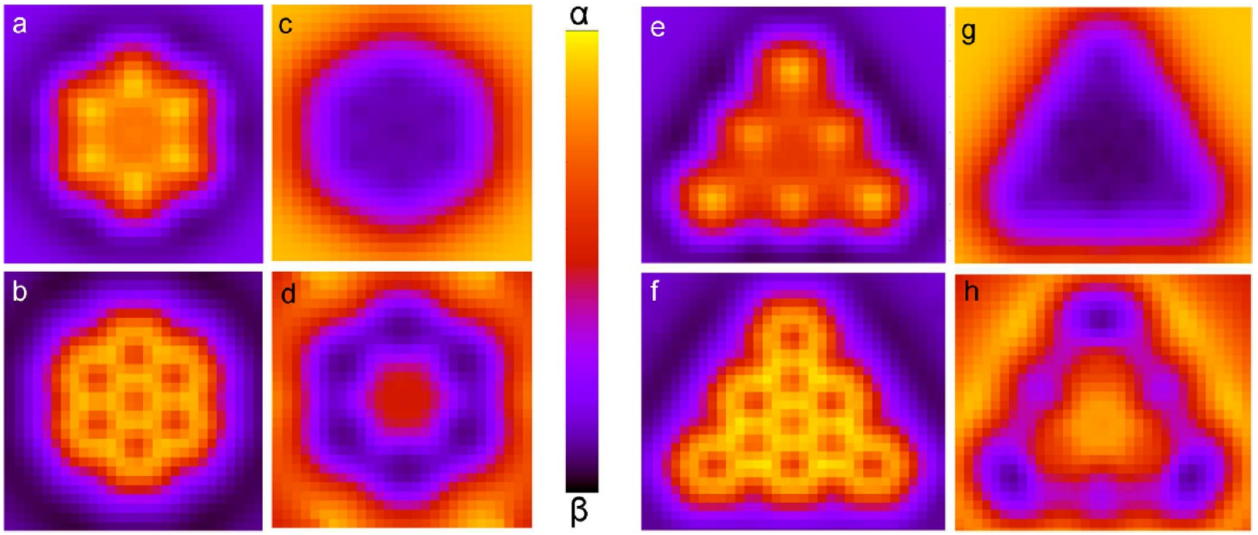

Figure 3. Scans of Cl^- (left) and Li^+ (right) above coronene (left set) and armchair-edge triangular H-passivated graphene flake (right set) at h = 2 Å (Cl^-) and 2.5 Å (Li^+) above the surface of each molecule. Potential energy surface for (a) Cl^- (α = −1374.94 au and β = −1375.1 au) and (c) Li^+ (α = −924.13 au and β = −924.22 au). Charge distribution surface for (b) Cl^- (α = −0.3 and β = −1.0) and (d) Li^+ (α = 1.0 and β = 0.78). Potential energy surface for (e) Cl^- (α = −1833.36 au and β = −1833.54 au) and (g) Li^+ (α = −1382.57 au and β = −1382.66 au). Charge distribution surface for (f) Cl^- (α = −0.3 and β = −1.0) and (h) Li^+ with α = 0.92 and β = 0.76.

edges. These expectations are confirmed in Figure 2c showing that when F^- is released at h = 4.8 Å (T = 300 K) it covalently binds within 1 ps to one of the C atoms at the (side) edge (sp^2 to sp^3 transition, see movie 4). However, when F^- is released at h < 2 Å above the flake, it binds to the nearest C atom (see movie 5). In experiments,[21,22] graphene fluorination was done with energetic ions (breaking of diatomic gas bonds by microwave or plasma) that prevent observation of different chemical functionalization at different graphene regions (bulk, edges).

Next, we present the results of F^- scanning at h = 2 Å above the armchair-edge triangular flake. Figure 2d indicates that the regions around the edge carbons (between the H atoms) again have a larger interaction energy (1.9 eV), but no preference to any particular region is observed. Figure 2e reveals that a large charge transfer (35%) occurs above most of the C atoms. Therefore, when F^- is released at h = 3.6 Å (T = 300 K) above the flake, it binds covalently to C atoms away from the edge (see Figure 2f). This preference in F^- binding to internal carbons might be caused by the edge deformation upon binding.[45]

3.3. Simulations of Other Ions. We also studied the coupling of other ions to graphene flakes. The simulations show that Cl^- covalently binds to larger zigzag and armchair triangular flakes, due to their increased polarization. Graphene chlorination has also been done in experiments.[27,28] We found that the system in Figure 2c is the smallest flake where covalent Cl^- binding can be observed. This indicates that polarization plays a significant role in chlorination of small graphene structures. On the other hand, Li^+ and Na^+ bind to triangular flakes by physisorption, as in coronene (Figure 1d−f).

In Figures 3a−d (left set), we show the results of scanning Cl^- (left) and Li^+ (right) ions at the height of h = 2 (Cl^-) and 2.5 Å (Li^+) above the surface of coronene. In Figures 3e−h (right set), the same is done above the surface of the armchair triangular flake in Figure 3f. As shown in Figures 3a and e, the interaction energy of Cl^- is weak at the center of both the coronene and the triangular flake, but it is stronger along the edges. The charge transfer surfaces for Cl^- above these flakes also follow the same pattern, with the highest transfer of ≈70% seen along the ring edges for both molecules (see Figures 3b and f). In contrast, Figures 3c and g show that Li^+ interacts more strongly with the central regions of both flakes, with a maximum energy difference between the edge and the center of ≈2.45 eV. In Figures 3d and h, we can see a charge transfer (≈23%) of a striking structure along the ring edges of both molecules. Here, the single-point calculations were performed at the B3LYP/3-21g* level with dispersion corrections (DFT-D3).

3.4. Porous Graphene Flakes. It is of large interest to study the dynamics of ions and molecules around nanopores formed in graphene, due to their numerous applications in nanofluidics, molecular separation, molecular detection, and energy storage.[31,35−38] Here, we describe coupling of ions to a rectangular H-passivated flake with a nanopore, shown in Figure 4 c. Scanning of F^- at h = 2 Å and Na^+ at h = 2.5 Å above the optimized flake is done with the single-point energies calculated at the RHF/3-21g level.

Figure 4 a presents the potential energy surface of F^- above the porous flake. Its minimum energy is at the zigzag-edge C atoms, about 4.9 eV deeper than in the pore area. The largest charge transfer also takes place over there (see Figure 4b). Although, this does not provide a direct evidence about the ion−flake covalent binding, we observe this binding of F^- to the zigzag edge of the regular flake (Figure 4f), when it is released at h = 6 Å and its trajectory is simulated for 1.5 ps at T = 300 K (B3LYP/6-31g level). When F^- is released at h < 3 Å above the regular flake, it covalently binds to any C atom. Its single-point energy scan with F^- at h = 2 Å gives similar results like in Figure 4a,b.

In Figure 4d, we also show the interaction energy of Na^+ to the porous flake. It has two large energy minima (≈3.3 eV) on the sides of the pore. Na^+ should physisorb to the porous flake as in the other structures. The charge transfer is relatively homogeneous across the whole structure, except for the large transfer at the pore region.

dx.doi.org/10.1021/jp400835w | J. Phys. Chem. C 2013, 117, 10750−10754

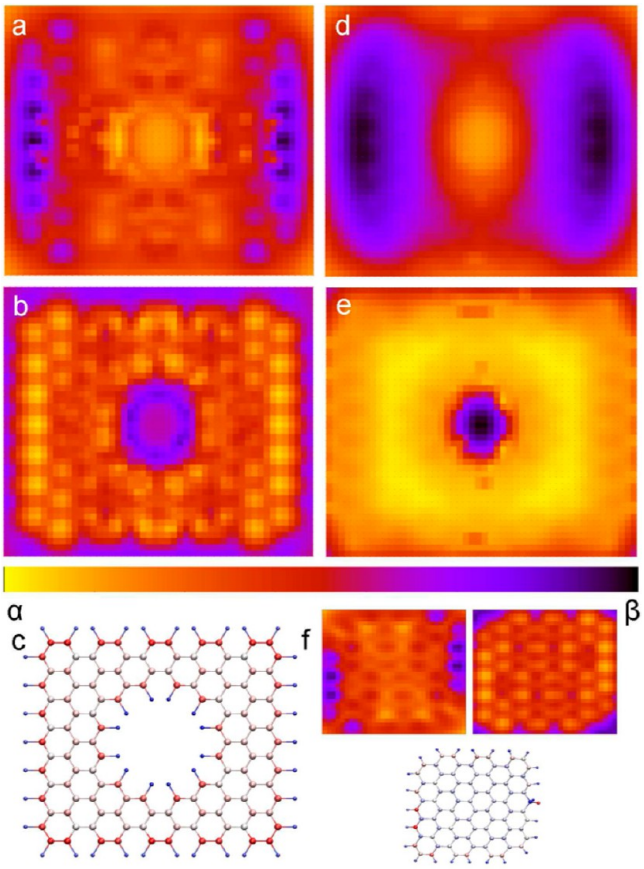

Figure 4. Scans of F^- (left) at h = 2 Å and Na^+ (right) at h = 2.5 Å above a rectangular H-passivated flake with a nanopore of the diameter ≈8.25 Å. Potential energy surface for (a) F^- (α = −4872.68 au and β = −4872.86 au) and (d) Na^+ (α = −4934.58 au and β = −4934.70 au). The charge transfer surface for (b) F^- (α = −0.45 and β = −1) and (e) Na^+ (α = 1 and β = 0.2). (c) The porous rectangular flake with atoms colored by charge. (f) Scanned calculations for a regular rectangular flake with F^-; (top left) potential energy surface (α = −3200.94 au and β = −3201.05 au); (top right) charge transfer surface (α = −0.45 and β = −0.95); (bottom) the rectangular flake with covalently bonded F^- at the edge, obtained after 1.5 ps quantum MD simulation at T = 300 K (F^- released at h ≈ 6 Å above the center of the flake).

3.5. Passage over the Nanostructure Edge. Above, we study ion coupling to a H-passivated nanopore with a diameter of 8.25 Å. Since nanopores used in practical systems can be relatively large (1−10 nm), here we briefly examine the passage of ions over the central part of the zigzag edge in the triangular H-passivated flake shown in Figure 2c. We scan Na^+ around the flake at the position of the central H atom, within 1.6 < h < 5 Å above the flake, at d > 0.7 Å in front of it. The calculations are done at the RHF/3-21g level.

Figure 5a shows the coupling energy between Na^+ and the flake. The energy is large at h = 3 Å above (below) the flake but rather small in front of it. We calculate the energy barrier for Na^+ to move from the top to the bottom of the flake (around the U-shape window in Figure 5), between a point located at h = 2 Å above the flake (7.5 Å from the left edge of Figure 5) and a point located at d = 1.45 Å in front of the H atoms within the plane of the flake. Since the barrier is E_b = 1.24 eV, the ion practically cannot overcome it at T = 300 K. Figure 3b also reveals that 0.3 e is passed to Na^+ close to the flake, as in coronene (Figure 1e), while at larger distances the charge transfer is fractional (limited validity).

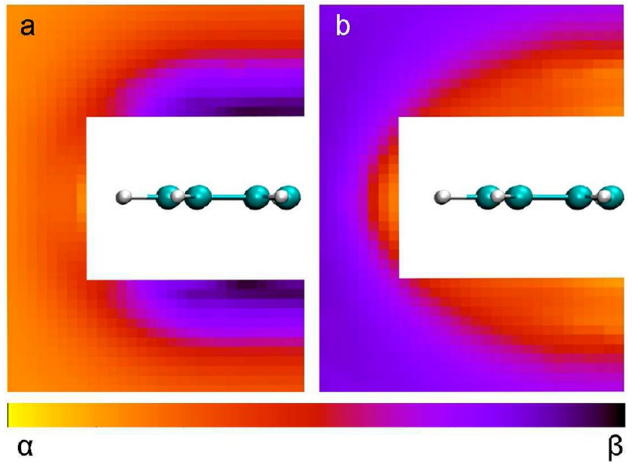

Figure 5. Scanning of Na^+ around the base of the zigzag-edge triangular H-passivated flake shown in Figure 2c (two basal layers of C rings are visualized from the structure). (a) The potential energy surface (α = −1915.39 au and β = −1915.47 au) and (b) the charge transfer surface (α = 1.1 and β = 0.4) are calculated in a U-shaped pixel arrangement around the flake (here, the pixel density is 0.25 Å).

4. CONCLUSIONS

We have studied the binding dynamics of monovalent ions to graphene-like H-passivated flakes. Our scanned ab initio calculations have revealed complex patterns in the potential energy and charge transfer surfaces of ions coupled to hexagonal, triangular, and porous graphene-based flakes. The scanned data correlate well with our time-dependent room-temperature quantum molecular dynamics simulations of the ion attachment to the graphene flakes. These studies open new avenues into large-scale exploration of nanoscale systems by first-principle methods.

■ ASSOCIATED CONTENT

Ⓦ Web-Enhanced Features

Movies are available in the HTML version of the paper.

■ AUTHOR INFORMATION

Corresponding Author

*Phone: (312) 996-6318. Fax: (312) 996-0431. E-mail: pkral@uic.edu.

Notes

The authors declare no competing financial interest.

■ ACKNOWLEDGMENTS

N.P. acknowledges the support from the Graduate Paaren Fellowship. The authors are grateful for allocation of computer time on the Forge Cluster at NCSA. We are also grateful to Henry Chan for his assistance with the simulation scripts.

■ REFERENCES

(1) Novoselov, K. S.; Geim, A. K.; Morozov, S. V.; Jiang, D.; Zhang, Y.; Dubonos, S. V.; Grigorieva, I. V.; Firsov, A. A. Electric Field Effect in Atomically Thin Carbon Films. *Science* **2004**, *306*, 666−669.

(2) Girit, C. Ö.; Meyer, J. C.; Erni, R.; Rossell, M. D.; Kisielowski, C.; Yang, L.; Park, C. H.; Crommie, M. F.; Cohen, M. L.; Louie, S. G.; et al. Graphene at The Edge: Stability and Dynamics. *Science* **2009**, *323*, 1705−1708.

(3) Wu, J.; Xie, L.; Li, Y.; Wang, H.; Ouyang, Y.; Guo, J.; Dai, H. Controlled Chlorine Plasma Reaction for Noninvasive Graphene Doping. *J. Am. Chem. Soc.* **2011**, *133*, 19668−19671.
(4) Klintenberg, M.; Lebegue, S.; Katsnelson, M. I.; Eriksso, O. Theoretical Analysis of the Chemical Bonding and Electronic Structure of Graphene Interacting With Group IA and Group VIIA Elements. *Phys. Rev. B* **2010**, *81*, 085433.
(5) Boukhvalov, D. W.; Katsnelson, M. I. Chemical Functionalization of Graphene. *J. Phys.: Condens. Matter* **2009**, *21*, 344205.
(6) Md., Zakir Hossain; Johns, J. E.; Bevan, K. H.; Karmel, H. J.; Liang, Y. T.; Yoshimoto, S.; Mukai, K.; Koitaya, T.; Yoshinobu, J.; Kawai, M.; et al. Chemically Homogeneous and Thermally Reversible Oxidation of Epitaxial Graphene. *Nature Chem.* **2012**, *4*, 305−309.
(7) Huang, B.; Li, Z. Y.; Liu, Z. R.; Zhou, G.; Hao, S. G.; Wu, J.; Gu, B. L.; Duan, W. H. Adsorption of Gas Molecules on Graphene Nanoribbons and Its Implication for Nanoscale Molecule Sensor. *J. Phys. Chem. C* **2008**, *112*, 13442−13446.
(8) Wang, Q. H.; Hersam, M. C. Room-Temperature Molecular-Resolution Characterization of Self-assembled Organic Monolayers on Epitaxial Graphene. *Nature Chem.* **2009**, *1*, 206−211.
(9) Geim, A. K.; Novoselov, K. S. The Rise of Graphene. *Nat. Mater.* **2007**, *6*, 183−191.
(10) Katsnelson, M. I. Graphene: Carbon in Two Dimensions. *Mater. Today* **2007**, *10*, 20−27.
(11) Castro Neto, A. H.; Guinea, F.; Peres, N. M. R.; Novoselov, K. S.; Geim, A. K. The Electronic Properties of Graphene. *Rev. Mod. Phys.* **2009**, *81*, 109−162.
(12) Liu, L.; Ryu, S.; Tomasik, M. R.; Stolyarova, E.; Jung, N.; Hybertsen, M. S.; Steigerwald, M. L.; Brus, L. E.; Flynn, G. W. Graphene Oxidation: Thickness-Dependent Etching and Strong Chemical Doping. *Nano Lett.* **2008**, *8*, 1965−1970.
(13) Byun, I. S.; Yoon, D.; Choi, J. S.; Hwang, I.; Lee, D. H.; Lee, M. J.; Kawai, T.; Son, Y. W.; Jia, Q.; Cheong, H.; et al. Nanoscale Lithography on Monolayer Graphene Using Hydrogenation and Oxidation. *ACS Nano* **2011**, *5*, 6417−6424.
(14) Si, Y.; Samulski, E. T. Synthesis of Water Soluble Graphene. *Nano Lett.* **2008**, *8*, 1679−1682.
(15) Elias, D. C.; Nair, R. R.; Mohiuddin, T. M. G.; Morozov, S. V.; Blake, P.; Halsall, M. P.; Ferrari, A. C.; Boukhvalov, D. W.; Katsnelson, M. I.; Geim, A. K.; et al. Control of Graphene's Properties by Reversible Hydrogenation: Evidence for Graphane. *Science* **2009**, *323*, 610−613.
(16) Balog, R.; Jørgensen, B.; Nilsson, L.; Andersen, M.; Rienks, E.; Bianchi, M.; Fanetti, M.; Lægsgaard, E.; Baraldi, A.; Lizzit, S.; et al. Bandgap Opening in Graphene Induced by Patterned Hydrogen Adsorption. *Nat. Mater.* **2010**, *9*, 315−319.
(17) Shytov, A. V.; Abanin, D. A.; Levitov, L. S. Long-Range Interaction Between Ad Atoms in Graphene. *Phys. Rev. Lett.* **2009**, *103*, 016806.
(18) Samarakoon, D. K.; Wang, X. Q. Tunable Band Gap in Hydrogenated Bilayer Graphene. *ACS Nano* **2010**, *4*, 4126−4130.
(19) Wu, M.; Tse, J. S.; Jiang, J. Z. Unzipping of Graphene by Fluorination. *J. Phys. Chem. Lett.* **2010**, *1*, 1394−1397.
(20) Medeiros, P. V. C.; Mascarenhas, A. J. S.; de Brito Mota, F.; de Catilho, C. M. C. A DFT Study of Halogen Atoms Adsorbed on Graphene Layers. *Nanotechnology* **2010**, *21*, 485701.
(21) Lee, W. H.; Suk, J. W.; Chou, H.; Lee, J.; Hao, Y.; Wu, Y.; Piner, R.; Akinwande, D.; Kim, K. S.; Ruoff, R. S. Selective-Area Fluorination of Graphene With Fluoropolymer and Laser Irradiation. *Nano Lett.* **2012**, *12*, 2374−2378.
(22) Yang, H.; Chen, M.; Zhou, H.; Qiu, C.; Hu, L.; Yu, F.; Chu, W.; Sun, S.; Sun, L. Preferential and Reversible Fluorination of Monolayer Graphene. *J. Phys. Chem. C* **2011**, *115*, 16844−16848.
(23) Bon, S. B.; Valentina, L.; Verdejo, R.; Fierro, J. L. G.; Peponi, L.; Lopez-Manchado, M. A.; Kenny, J. M. Plasma Fluorination of Chemically Derived Graphene Sheets and Subsequent Modification With Butylamine. *Chem. Mater.* **2009**, *21*, 3433−3438.
(24) Ribas, M. A.; Singh, A. K.; Sorokin, P. B.; Yakobson, B. I. Patterning Nanorods and Quantum Dots on Fluorinated Graphene. *Nano Res.* **2011**, *4*, 143−152.
(25) Robinson, J. T.; Burgess, J. S.; Junkermeier, C. E.; Badescu, S. C.; Reinecke, T. L.; Perkins, K. F.; Zalalutdniov, M. K.; Baldwin, J. W.; Culbertson, J. C.; Sheehan, P. E.; et al. Properties of Fluorinated Graphene Films. *Nano Lett.* **2010**, *10*, 3001−3005.
(26) Yang, M.; Zhou, L.; Wang, J.; Liu, Z.; Liu, Z. Evolutionary Chlorination of Graphene: From Charge-Transfer Complex to Covalent Bonding and Nonbonding. *J. Phys. Chem. C* **2012**, *116*, 844−850.
(27) Li, B.; Zhou, L.; Wu, D.; Peng, H.; Yan, K.; Zhou, Y.; Liu, Z. F. Photochemical Chlorination of Graphene. *ACS Nano* **2011**, *5*, 5957−5961.
(28) Zhang, L.; Yu, J.; Yang, M.; Xie, Q.; Peng, H.; Liu, Z. Janus Graphene from Asymmetric Two-dimensional Chemistry. *Nat. Commun.* **2013**, *4*, 1443.
(29) Zheng, J.; Liu, H. T.; Wu, B.; Di, C. A.; Guo, Y. L.; Wu, T.; Yu, G.; Liu, Y. Q.; Zhu, D. B. Production of Graphite Chloride and Bromide Using Microwave Sparks. *Sci. Rep.* **2012**, *2*, 662.
(30) Nakada, K.; Fujita, M.; Dresselhaus, G.; Dresselhaus, M. S. Edge State in Graphene Ribbons: Nanometer Size Effect and Edge Shape Dependence. *Phys. Rev. B* **1996**, *54*, 17954.
(31) Sint, K.; Wang, B.; Král, P. Selective Ion Passage Through functionalized Graphene Nanopores. *J. Am. Chem. Soc.* **2008**, *130*, 16448−16449.
(32) Stoller, M. D.; Park, S.; Zhu, Y.; An, J.; Ruoff, R. S. Graphene-based Ultracapacitors. *Nano Lett.* **2008**, *8*, 3498−3502.
(33) Loh, K. P.; Bao, Q.; Eda, G.; Chhowalla, M. Graphene Oxide as a Chemically Tunable Platform for Optical Applications. *Nature Chem.* **2010**, *2*, 1015−1024.
(34) Baskin, A.; Král, P. Electronic Structures of Porous Nanocarbons. *Sci. Rep.* **2011**, *1*, 36.
(35) Blankenburg, S.; Bieri, M.; Fasel, R.; Müllen, K.; Pignedoli, C. A.; Passerone, D. Porous Graphene as an Atmospheric Nanofilter. *Small* **2010**, *6*, 2266−2271.
(36) Garaj, S.; Hubbard, W.; Reina, A.; Kong, J.; Branton, D.; Golovchenko, J. Graphene as a Subnanometre Trans-Electrode Membrane. *Nature* **2010**, *467*, 190−193.
(37) Nair, R. R.; Wu, H. A.; Jayaram, P. N.; Grigorieva, I. V.; Geim, A. K. Unimpeded Permeation of Water Through Helium-Leak-Tight Graphene-Based Membranes. *Science* **2012**, *335*, 442−444.
(38) Merlet, C.; Rotenberg, B.; Madden, P. A.; Taberna, P. L.; Simon, P.; Gogotsi, Y.; Salanne, M. On the Molecular Origin of Supercapacitance in Nanoporous Carbon Electrodes. *Nat. Mater.* **2012**, *11*, 306−310.
(39) Gross, L.; Mohn, F.; Moll, N.; Schuler, B.; Criado, A.; Guitian, E.; Pena, D.; Gourdon, A.; Meyer, G. Bond-Order Discrimination by Atomic Force Microscopy. *Science* **2012**, *337*, 1326−1329.
(40) Ufimtsev, I. S.; Martinez, T. J. Quantum Chemistry of Graphical Processing Units. 3. Analytical Energy Gradients, Geometry Optimization and First Principles Molecular Dynamics. *J. Chem. Theory Comput.* **2009**, *5*, 2619−2628.
(41) Grimme, S.; Antony, J.; Ehrlich, S.; Krieg, H. A. A Consistent and Accurate ab initio Parametrization of Density Functional Dispersion Correction (DFT-D) for the 94 Elements H-Pu. *J. Chem. Phys.* **2010**, *132*, 154104.
(42) Grimme, S.; Ehrlich, S.; Goerigk, L. Effect of the Damping Function in Dispersion Corrected Density Functional Theory. *J. Comput. Chem.* **2011**, *32*, 1456−1465.
(43) Polo, V.; Kraka, E.; Cremer, D. Electron Correlation and the Self-Interaction Error of Density Functional Theory. *Mol. Phys.* **2002**, *100*, 1771−1790.
(44) Kästner, J.; Carr, J. M.; Keal, T. W.; Thiel, W.; Wander, A.; Sherwood, P. DL-FIND: An Open-Source Geometry Optimizer for Atomistic Simulations. *J. Phys. Chem. A* **2009**, *113*, 11856−11865.
(45) Lee, H. Preferential Functionalization on Zigzag Graphene Nanoribbons: First-Principles Calculations. *J. Phys.: Condens. Matter* **2010**, *22*, 352205.